# The Mechanism of Copper-Catalyzed Trifunctionalization of Terminal Allenes

Hong Ki Kim, [a,b] Manoj V. Mane, [b,a] John Montgomery, \*[c] and Mu-Hyun Baik\*[b,a]

#### **ABSTRACT**

A highly selective copper-catalyzed trifunctionalization of allenes has been established based on diborylation/cyanation with bis(pinacolato)diboron ( $B_2pin_2$ ) and N-cyano-N-phenyl-p-toluenesulfonamide (NCTS). The Cu-catalyzed trifunctionalization of terminal allenes is composed of three catalytic reactions ( $1^{st}$  borocupration, electrophilic cyanation and  $2^{nd}$  borocupration) that provide a densely functionalized product with regio-, chemo- and diastereoselectivity. Allene substrates have multiple reaction-sites, and the selectivities are determined by the suitable interactions (e.g. electronic and steric demands) between the catalyst and substrates. We employed density functional theory (DFT) calculations to understand the cascade copper-catalyzed trifunctionalization of terminal allenes, providing densely-functionalized organic molecules with outstanding regio-, chemo- and diastereoselectivity in high yields. Systematic computational studies for the high selectivity levels seen give insight into the design of catalytic multiple-functionalization strategies that address the selectivity challenges presented by cumulated  $\pi$ -systems.

[a] H. K. Kim, Dr. M. V. Mane, Prof. Dr. M.-H. Baik

Department of Chemistry

Korea Advanced Institute of Science and Technology (KAIST)

Daejeon 34141 (Republic of Korea)

E-mail: mbaik2805@kaist.ac.kr

[b] H. K. Kim, Dr. M. V. Mane, Prof. Dr. M.-H. Baik

Center for Catalytic Hydrocarbon Functionalizations, Institute for Basic Science (IBS)

Daejeon 34141 (Republic of Korea)

[c] Prof. Dr. J. Montgomery

Department of Chemistry

University of Michigan

930 North University Avenue, Ann Arbor, Michigan 48109-1055, (United States)

Email: imontg@umich.edu

# INTRODUCTION

Transition-metal-catalyzed functionalization of boron-containing σ-bonds to carbon–carbon multiple bonds is an effective strategy for the formation of densely functionalized organic molecules.<sup>[1]</sup> In particular, transition-metal boryl complexes play a key role in a range of borylation reactions such as C–H borylation, hydroboration, diboration, and other B–X addition reactions on unsaturated organic substrates.<sup>[1f,2]</sup> More specifically, allene substrates have been investigated previously, motivated by the variety of structural motifs and functional value that allenes present for access to natural products, pharmaceuticals, and organic materials.<sup>[2e,2f,3]</sup> Trifunctionalization processes have the potential to provide practical and powerful solutions for accessing valuable organic molecules with intriguing selectivities and high yields,<sup>[1b–e,4]</sup> but the strategy remains underdeveloped compared to other reaction types that show similar versatility. Recently, Ma and Ito reported the borocupration reaction of allenes with B<sub>2</sub>pin<sub>2</sub> based on both experimental and theoretical studies.<sup>[5]</sup> Furthermore, although the borometallation processes of substrates that possess two or more unsaturations have considerable potential in this regard, but their application in trifunctionalization processes has seen very limited exploration.

Recently, one of us reported that a copper-catalyzed cascade trifunctionalization of terminal allenes derived from diborylation and cyanation provides a method to efficiently synthesize functionalized products with high degrees of regio-, chemo- and diastereoselectivity, as depicted in **Scheme 1**.<sup>[6]</sup> Based on our previous experimental study, a putative mechanism was proposed to involve a series of diborylation and cyanation on the  $\pi$ -systems of the allene substrates. Most importantly, we were able to isolate an alkenyl intermediate, which is proposed to give the trifunctionalized final product. Whereas the overall sequence of the reaction appears to be clear, many important details remain poorly understood. For example, it is not at all clear which features govern the various selectivities that have been observed and that make these reactions synthetically attractive.

Scheme 1. Cascade Copper-Catalyzed Trifunctionalization Process: A Triple-Selective Functionalization of Cyclohexyl Allene.

In this study, we employed density functional theory (DFT) calculations to understand the mechanism for the copper-catalyzed trifunctionalization of cyclohexyl allene in detail. The aim of this study is to explain the observed triple-selectivities as shown in **Scheme 1** and to construct a complete mechanistic framework that will offer mechanistic details to expedite the rational design of the next generation of new catalytic reactions.

#### **COMPUTATIONAL METHODS**

All calculations were performed using density functional theory<sup>[7]</sup> (DFT) as implemented in the Jaguar 9.1 suite<sup>[8]</sup> of ab initio quantum chemistry programs. Geometry optimizations to the stationary points as well as the transition state (TS) optimization to the saddle points were performed the B3LYP<sup>[9]</sup> hybrid exchange and correlation functional including Grimme's D3 dispersion correction.<sup>[10]</sup> The 6-31G\*\* basis set<sup>[11]</sup> was used for all atoms except for copper, which was represented by the Los Alamos LACVP\*\* basis set<sup>[12]</sup> including effective core potentials. The

energies of the optimized structures were reevaluated by single-point calculations on each optimized geometry using Dunning's correlation consistent triple- $\zeta$  basis set cc-pVTZ(-f)<sup>[13]</sup> that includes a double set of polarization functions. Copper were represented using a triple- $\zeta$  version of LACVP\*\*, where the exponent of the basis functions were decontracted to mimic the flexibility of the triple- $\zeta$  basis. Analytical vibrational frequencies within the harmonic oscillator approximation were computed with the B3LYP-D3/6-31G\*\* level to confirm proper convergence to well-defined minima and saddle points on the potential energy surface. Solvation energies were evaluated by a self-consistent reaction field (SCRF) approach based on accurate numerical solutions of the Poisson–Boltzmann equation. These solvation calculations were carried out with the B3LYP-D3/6-31G\*\* level at the optimized gasphase geometry employing the dielectric constant of  $\varepsilon = 7.6$  for tetrahydrofuran (THF). As is the case for all continuum models, the solvation energies are subject to empirical parametrization of the atomic radii that are used to generate the solute surface. We employed the standard set of optimized radii in Jaguar for H (1.150 Å), B (2.042 Å), C (1.900 Å), N (1.600 Å), Na (1.600 Å), Na (1.491 Å), S (2.070 Å), Cl (1.974 Å) and Cu (1.748 Å). The free energy in solution-phase G(sol) has been calculated as follows:

$$G(sol) = G(gas) + \Delta G(solv)$$
 (1)

$$G(gas) = H(gas) - TS(gas)$$
 (2)

$$H(gas) = E(SCF) + ZPE$$
 (3)

$$\Delta E(SCF) = \Sigma E(SCF)$$
 for products –  $\Sigma E(SCF)$  for reactants (4)

$$\Delta G(sol) = \Sigma G(sol)$$
 for products –  $\Sigma G(sol)$  for reactants (5)

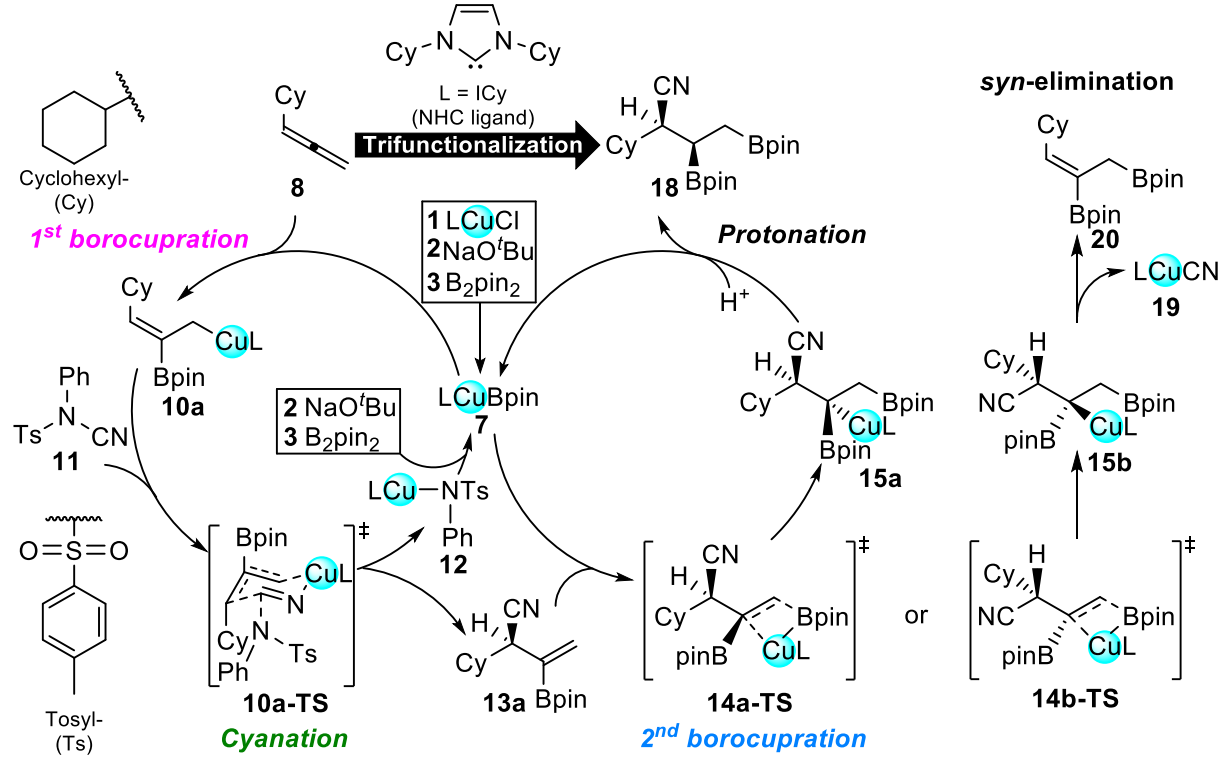
G(gas) is the free energy in the gas-phase; G(solv) is the free energy of solvation as computed using the continuum solvation model; H(gas) is the enthalpy in gas-phase; T is the temperature (298.15 K); S(gas) is the entropy in the gas-phase; E(SCF) is the self-consistent field energy, i.e., raw electronic energy as computed from the SCF procedure; and ZPE is the zero-point energy. Note that by entropy here we refer specifically to the vibrational/translational entropy of the solute(s); the entropy of the solvent is incorporated implicitly in the continuum solvation model. Transition state structures were obtained from the quadratic synchronous transit (QST) search methods.<sup>[16]</sup>

### **Results and Discussion**

**Mechanism.** The proposed reaction pathway for the Cu(I)-catalyzed trifunctionalization of the allene substrate is outlined in **Scheme 2** and consists of three major steps that govern the regio-, chemo- and diastereoselectivities. For the purpose of constructing a model reaction energy profile, which is shown in **Figure 2**, we chose to employ the cyclohexyl allene substrate, which was experimentally shown to selectively form the 1,2,3-trifunctionalized product **18** in high yields. In general, borocupration reactions are thought to involve *N*-heterocyclic carbene (NHC) copper-boryl complex **7** as the active species with a range of reported NHC ligands such as 1,3-bis(2,4,6-trimethylphenyl)- 4,5-dihydroimidazol-2-ylidene

(SiMes), 1,3-*bis*(2,6-diisopropylphenyl)imidazol-2-ylidene (IPr), and 1,3-dicyclohexylimidazol-2-ylidene (ICy).<sup>[17]</sup> Among them, ICy was found to offer the best combination of high yields and triple-selectivities for the product **18**. The catalytic cycles proceed as summarized in **Scheme 2**, with the pre-catalyst ICyCu–Cl, B<sub>2</sub>pin<sub>2</sub>, and NaO<sup>t</sup>Bu reacting to generate ICyCu–Bpin species **7** in tetrahydrofuran (THF) as a solvent.

Scheme 2. Overview of Mechanism for Cu-Catalyzed Trifunctionalization of Cyclohexyl Allene.



The formation of the catalytically active species **7** deserves some attention, as it is the key intermediate that starts the catalytic cycle and is responsible for two different borylation cycles during the reaction cascade. It is generated from the pre-catalyst LCu–Cl with NaO'Bu and B<sub>2</sub>Pin<sub>2</sub>, as illustrated in **Figure 1**.<sup>[18]</sup> Starting from reactants **1** and **2**, ligand exchange gives a thermodynamically stable LCu–O'Bu complex **5** and sodium chloride, which can undergo a  $\sigma$ -bond metathesis reaction where the Cu–O and B–B bonds are cleaved and Cu–B and O–B bonds are formed through a typical four-membered transition state **3-TS** at a relative energy of 16.2 kcal/mol to afford the stable intermediate complex **7** at –15.6 kcal/mol. We expect this reaction to be irreversible and rapid given the low barrier and large exothermic driving force.

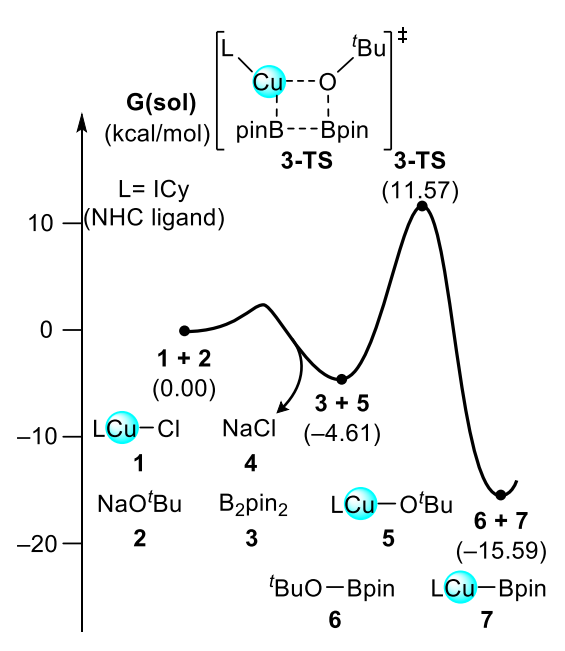


Figure 1. Energy profiles for pre-catalyst activation.

As illustrated in Figure 2, the catalytic cycle starts with species 7 adding across a terminal double bond of the allene to form an intermediate **9a**, a Cu- $\eta^2$ -allene  $\pi$ -complex, at a relative energy of 4.6 kcal/mol, making this step endergonic by 11.0 kcal/mol. The insertion of the allene into the Cu–B bond is surprisingly easy from this πadduct only requiring an additional 7.7 kcal/mol to afford an overall barrier 18.7 kcal/mol for the insertion from intermediate 7. The inserted species is the olefin intermediate 10a, which we were able to locate at -45.4 kcal/mol, rendering this insertion step highly irreversible. Note that the regiochemical outcome of which double bond of the allene is functionalized is determined at this step, as will be discussed in greater detail below. Our calculations suggest that intermediate 10a should not be experimentally observable, because the next step, which is the cyanation, is associated with a very low barrier of only 13.9 kcal/mol traversing the transition state 10a-TS. Orthocyanation of a benzyl copper species by reagent 11 was first described by Buchwald[19] and was computationally studies by Liu. [20] Given that the cyanating reagent is offered in sufficient quantities, this step is expected to be fast, preventing the accumulation of 10a in the reaction mixture. The product of the cyanation is intermediate 13a, located at a free energy of -83.5 kcal/mol, rendering the cyanation step also irreversible with an energetic driving force of 10a → 13a to be 38.1 kcal/mol. For the final step of the cascade reaction, intermediate 13a must be re-engaged by the catalytically active species 7 to facilitate the second borocupration reaction. Our calculations suggest that this step is also facile with a step barrier of only 11.4 kcal/mol associated with the transition state 14a-TS to give the product complex 15a, but since the concentration of 7 is low, the rate of this step is expected to be low compared to the other steps with similar or even slightly higher barriers. As a consequence, the alkenyl intermediate 13a may accumulate during the catalytic reaction and become amenable for isolation, as was previously found. Furthermore, we observed independently-prepared compound 13a is converted to the expected product 18 experimentally, and suggested that 13a is not the final product because 2nd borocupration is a highly exothermic reaction with an energetic driving force of 15.7 kcal/mol and the lowest activation barrier of about 11 kcal/mol in the copper-catalyzed trifunctionalization reaction based on DFT calculations. Finally, protonation of 15a gives the trifunctionalized cyanation/diborylation product 18. Figure 2 also indicates which step is responsible for the regio-, chemo- and

diastereoselectivity, namely, the first borylation, the cyanation and the second borylation steps, respectively. These features are discussed in detail below.

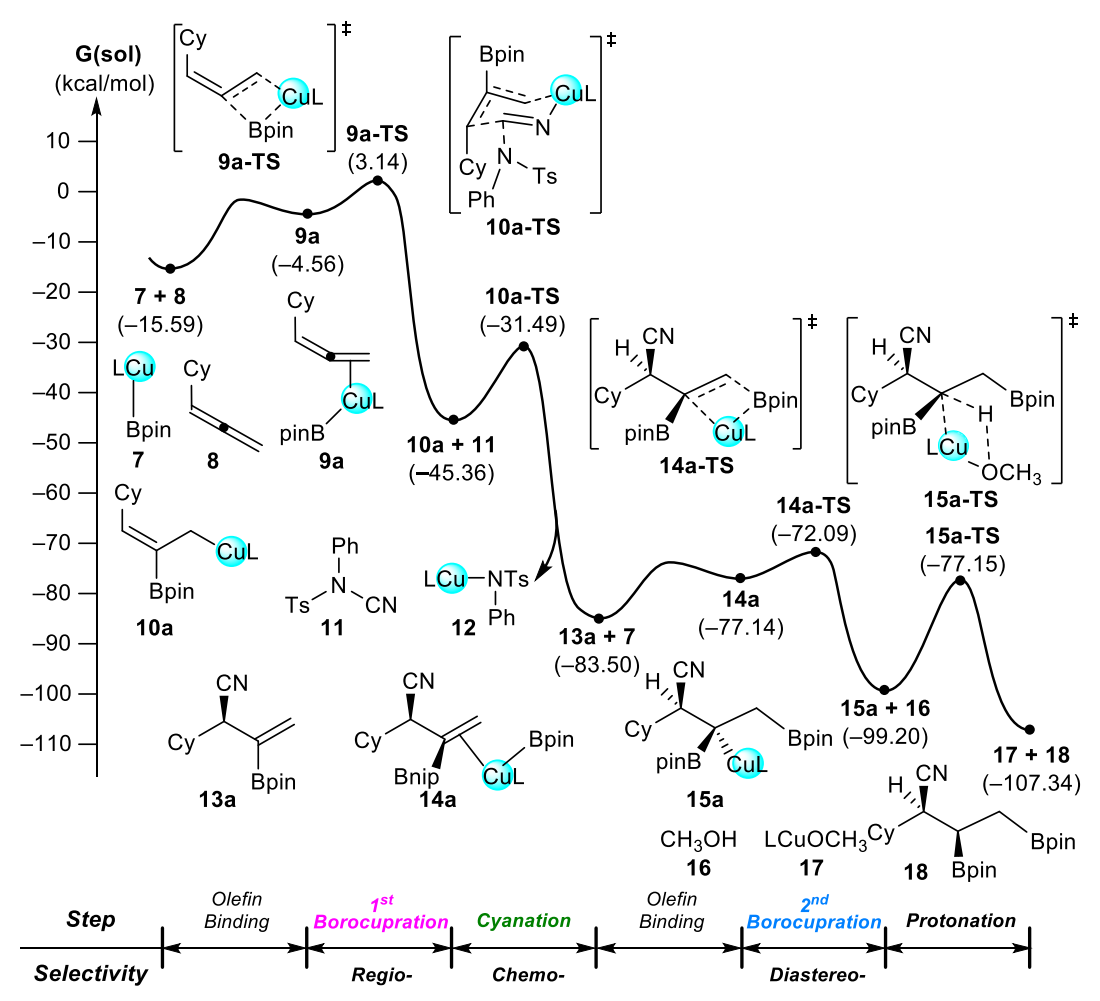
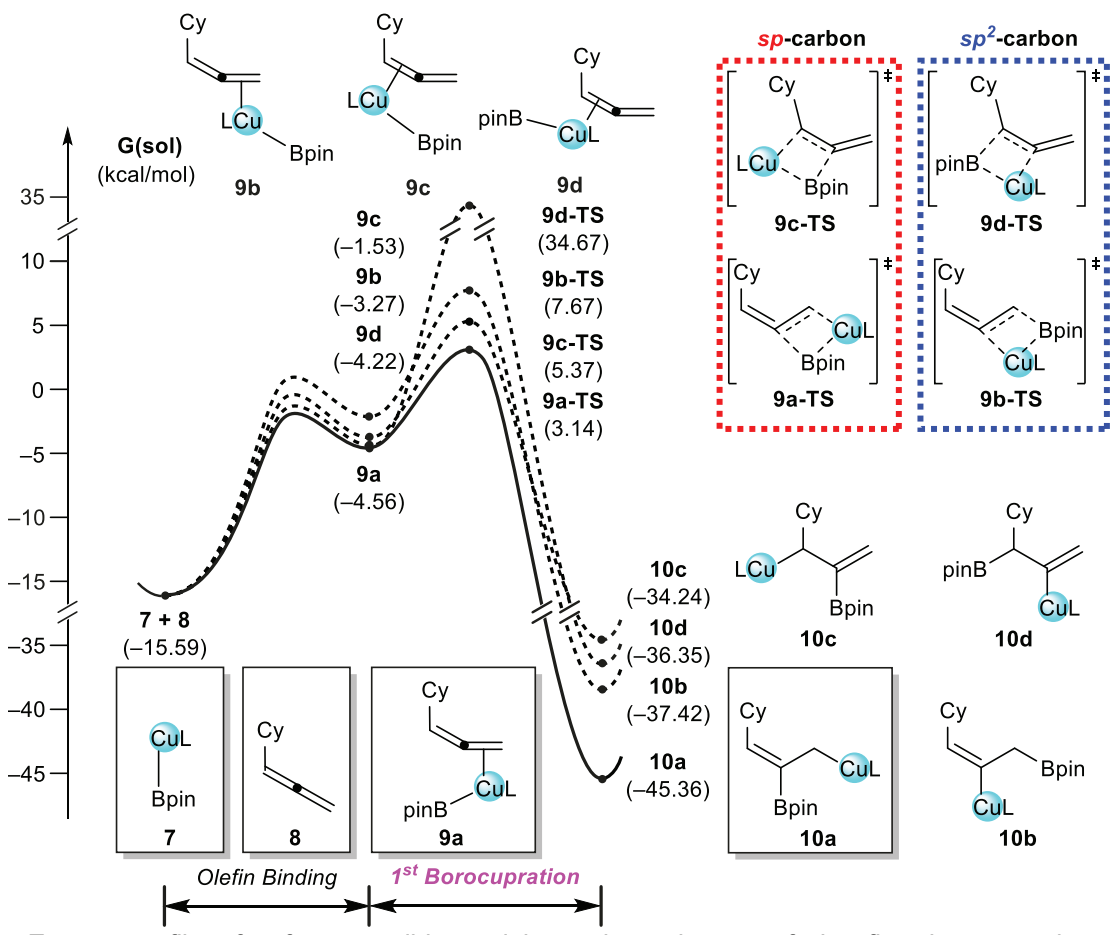


Figure 2. Overall energy profiles for Cu-catalyzed trifunctionalization of terminal allenes.

Regioselective First Borocupration. As discussed above, the first borocupration of the allene substrate determines the regioselectivity in the cascade reaction. In principle, there are four possible ways of inserting the cyclohexyl allene substrate 8 into the Cu–B bond, as summarized in Figure 3. Within an energy range of ~3 kcal/mol, we were able to locate four structural isomers of the reactant π-complex, where 9a and 9b have the copper-catalyst bound at the distal double bond from the cyclohexyl group adopting two different orientations of the NHC-ligand. Intermediates 9c and 9d are the analogous π-complexes where the Cu engages the proximal double bond. These four structural isomers offer entries into the four different regiochemical reaction channels that will produce regioisomeric borocupration products 10(a–d), as illustrated in Figure 3. The barriers associated with these four channels and the transition states 9(a–d)-TS are remarkably different at 18.7, 21.0, 23.3 and 50.3 kcal/mol, respectively. The trajectory with the lowest barrier associated with 9a-TS gives intermediate 10a, which is also the lowest in energy by ~8-11 kcal/mol among all regioisomers at –45.4 kcal/mol.



**Figure 3.** Energy profiles for four possible regioisomeric pathways of the first borocupration related to regioselectivity.

To understand the origin of the regioselectivity during the first borocupration, we examined each transition state 9(a-d)-TS on the four different regiochemical reaction channels. This analysis illustrated that there are two features that determine the energies of these transition states. First, the insertion of the boryl moiety to form the C-B bond favors the stronger Lewis basic sp-carbon of the allene over the weaker Lewis basic sp-carbon as highlighted in **Figure 3**. This finding is easy to understand since the boryl group acts as a Lewis acid in this bond formation. Thus, the transition states 9a-TS and 9c-TS are electronically favored over transition states 9b-TS and 9d-TS. The second determining factor is the steric demand enforced by the cyclohexyl functionalities flanking the N-heterocyclic ligand and the terminal cyclohexyl groups of the allene substrate. As depicted in **Figure 4**, these sterically demanding groups are oriented away from each other in 9a-TS and 9b-TS. In the other two transition states, the cyclohexyl groups cause a steric clash, giving rise to higher energies. Consequently, 9a-TS is lowest in energy. For similar reasons, intermediate 10a is about 8 kcal/mol lower in energy than 10b. Therefore, the formation of the  $\sigma$ -allyl complex 10a is kinetically and thermodynamically most affordable.

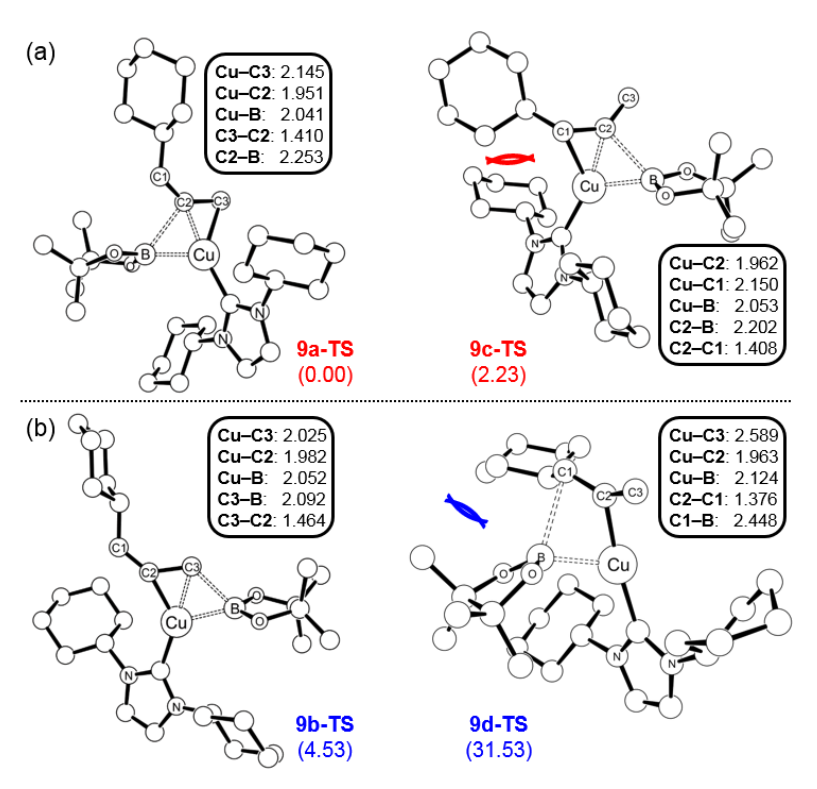


**Figure 4.** For the first borocupration, four possible transition state structures forming the C–B bond related to sp-carbon (a) and sp<sup>2</sup>-carbon (b). Hydrogen atoms bound to carbon atoms are omitted for the sake of clarity. All bond lengths are in Å. Relative free energy differences (kcal/mol) are in parenthesis.

Stereoselective Cyanation. After undergoing the borocupration, the NCTS substrate can act as an electrophilic cyanating agent to afford cyanation products in high yield with excellent selectivity. [19–21] As shown in Figure 5, the step barrier associated with 10a-TS is only 14.0 kcal/mol that is expected to be fast in realistic reaction conditions, and the transition state adopts a six-membered ring conformation as the copper center coordinates to the terminal nitrogen atom of the cyano group. Consequently, placing the cyclohexyl group in the axial position allows for a relaxed geometry via six-membered without steric stress. Furthermore, we found the two possible conformational isomers 13a and 13b that may be formed from intermediate 11 via transition state 10a-TS. The rotamers 13a and 13b were transferable to the experimentally observed stereoselectivity in the second borocupration step.

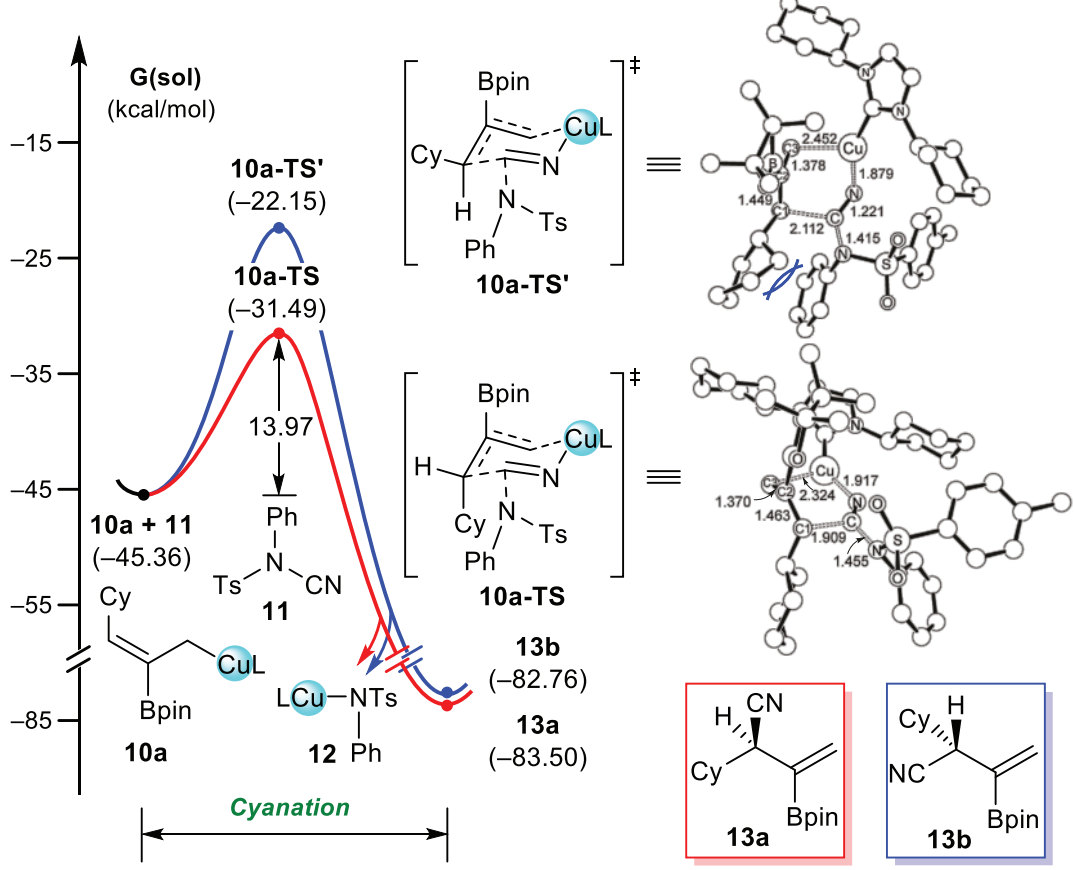


**Figure 5.** Energy profiles of cyanation pathway. Hydrogen atoms bound to carbon atoms are omitted for the sake of clarity. All bond lengths are in Å.

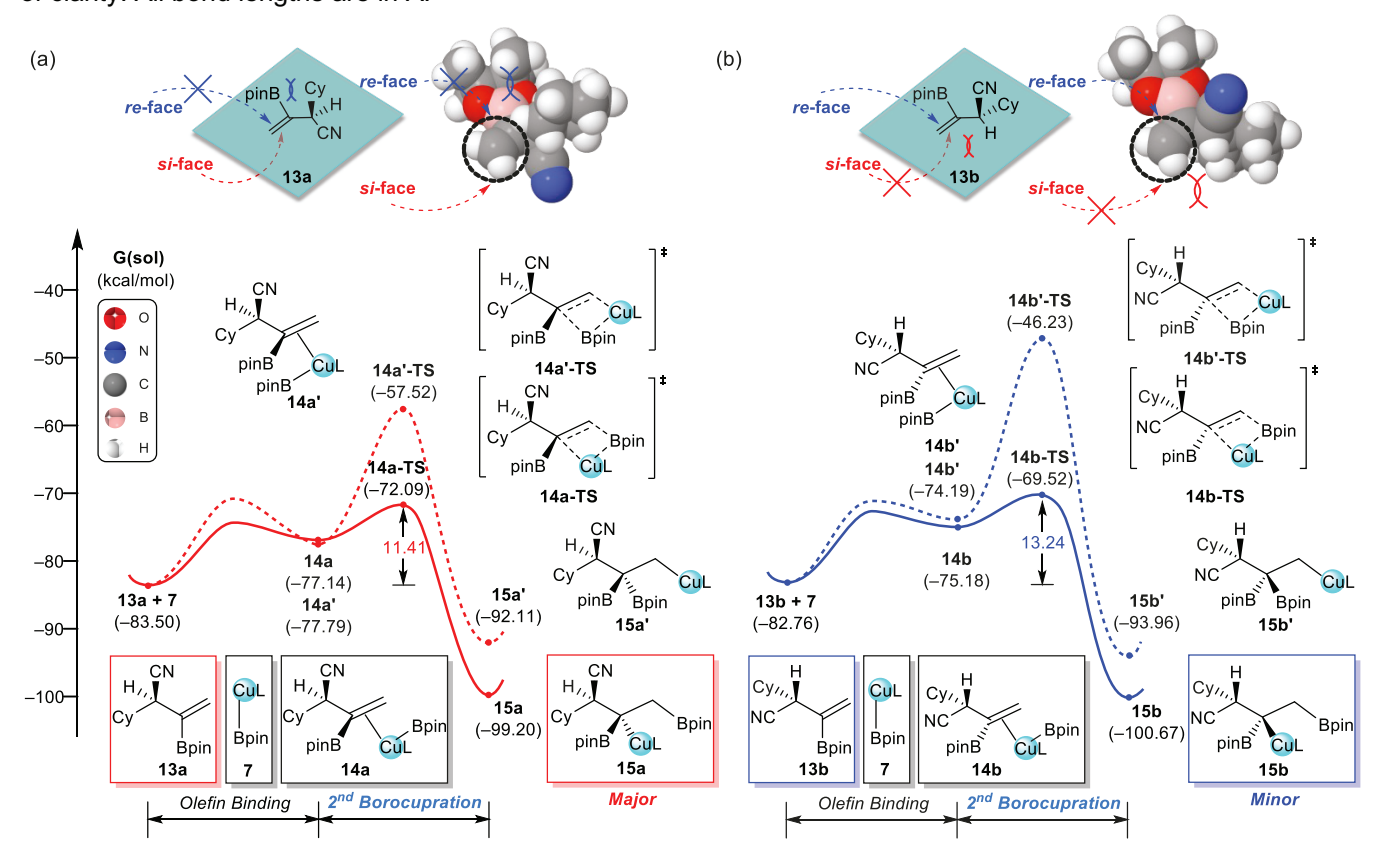


**Figure 6.** Energy profiles for the second borocupration pathways related to regio- and diastereoselectivity derived from two conformational isomers 13a and 13b.

Regio- and Diastereoselective Second Borocupration. The addition of boryl copper 7 to the olefin occurs in a regio- and stereoselective manner. The stereocontrol is imposed by the sterically demanding interaction between the cyclohexyl group of the alkene substrate and species 7. As illustrated in Figure 6a, the boryl copper complex 7 reacts with 13a on the si-face because the cyclohexyl group effectively blocks the re-face. Conversely, in 13b the re-face is blocked by the cyclohexyl moiety, forcing the borocupration to proceed through the si-face depicted in Figure 6b. Four borocuparated products 15a, 15b, 15a' and 15b' are possible, as shown in Figures 6 and Figure S1. The intermediate 13a first forms the π-complex with 7, which is ~6 kcal/mol uphill to afford the two conformers 14a and 14a'. The borocupration is exceedingly facile and reaching 14a-TS only requires an addition 5 kcal/mol to give a total barrier of only 11.4 kcal/mol and form product 15a. The reaction leading to the alternative regioisomer 15a' is much more difficult and associated with a barrier of 19.6 kcal/mol. This regiochemical outcome is easy to understand, as the double-bond is likely cleaved in a heterolytic fashion with the terminal carbon becoming negatively polarized, which is well matched with the boryl functionality, which acts as a Lewis acid. The regiocontrol is also operative for the intermediates 14b and 14b', thus, favoring the formation of 15b with a barrier of 13.2 kcal/mol. Comparing the diastereoisomers 15a and 15b, our calculations predict a nearly 2 kcal/mol kinetic preference for the formation of 15a, which is again in excellent agreement with experimental observations. As discussed above, protonation of 15a affords the final trifunctionalized product 18.

#### **Conclusions**

In summary, our calculations have revealed a detailed mechanism for the Cu-catalyzed trifunctionalization of cyclohexyl allene employing B<sub>2</sub>pin<sub>2</sub> and NCTS as the borylation and cyanation source. We present for the first time how this fascinating, efficient cascade reaction that generated the cyanation/diborylation product with exceptional regio-, chemo- and diastereoselectivity can be understood in detail. Although the sequence of the three reactions occurs in a highly orchestrated fashion, the regio- and stereoselectivities determined in each of the reaction steps are easily rationalized by this study. Specifically, the regiocontrol of the two borocupration steps is determined by significantly different effects. The first borocupration employs mostly sterical demands, but the second borocupration utilizes mainly electronic effects. The diastereoselectivity follows a classical strategy of sterical blocking one of the reactive faces of the olefin by placing the cyclohexyl functionality in that molecular face. This detailed mechanistic investigation offers a precise mechanistic blueprint and serves as a platform for future explorations and rational catalyst design efforts. Applications of these design concepts will be pursued in our laboratories and reported in due course.

## **Supporting Information**

For computed energy components, Cartesian coordinates, vibrational frequencies of all of the DFT-optimized structures, see Supporting Information.

#### **ORCID**

Hong Ki Kim: 0000-0002-6115-384X Manoj V. Mane: 0000-0001-8236-3638 John Montgomery: 0000-0002-2627-2317 Mu-Hyun Baik: 0000-0002-8832-8187

#### Acknowledgment

We thank the Institute for Basic Science (IBS-R10-A1) in Korea and the US National Science Foundation (CHE-1565837) for financial support.

#### **Conflicts of interest**

The authors declare no competing financial interest.

**Keywords:** density functional theory · trifunctionalization · borylation · cyanation · copper catalysis · selectivities

### Reference

- a) N. F. Pelz, J. P. Morken, *Org. Lett.* 2006, *8*, 4557–4559; b) G. R. Clark, P. M. Johns, W. R. Roper, T. Söhnel, L. James Wright, *Organometallics* 2011, *30*, 129–138; c) Q. Feng, K. Yang, Q. Song, *Chem. Commun.* 2015, *51*, 15394–15397; d) Y. Li, D. Qiu, R. Gu, J. Wang, J. Shi, Y. Li, *J. Am. Chem. Soc.* 2016, *138*, 10814–10817; e) S. Ni, W. Sha, L. Zhang, C. Xie, H. Mei, J. Han, Y. Pan, *Org. Lett.* 2016, *18*, 712–715; f) K. Semba, M. Shinomiya, T. Fujihara, J. Terao, Y. Tsuji, *Chem. Eur. J.* 2013, *19*, 7125–7132.
- [2] a) S. Ma, Acc. Chem. Res. 2009, 42, 1679–1688; b) R. Zimmer, C. U. Dinesh, E. Nandanan, F. A. Khan, Chem. Rev. 2000, 100, 3067–3126; c) S. Ma, Acc. Chem. Res. 2003, 36, 701–712; d) S. Ma, Chem. Rev. 2005, 105, 2829–2872; e) N. Krause, C. Winter, Chem. Rev. 2011, 111, 1994–2009; f) S. Yu, S. Ma, Angew. Chem. Int. Ed. 2012, 51, 3074–3112; g) R. K. Neff, D. E. Frantz, Tetrahedron 2015, 71, 7–18.
- [3] a) A. S. Hashmi, Angew. Chem. Int. Ed. 2000, 39, 3590–3593; b) J. A. Marshall, K. G. Pinney, J. Org. Chem. 1993, 58, 7180–7184; c) J. A. Marshall, G. S. Bartley, E. M. Wallace, J. Org. Chem. 1996, 61, 5729–5735; d) K. Yeung, F. J. T. Talbot, G. P. Howell, A. P. Pulis, D. J. Procter, ACS Catal. 2019, 1655–1661.
- [4] a) X.-Y. Duan, X.-L. Yang, R. Fang, X.-X. Peng, W. Yu, B. Han, J. Org. Chem. 2013, 78, 10692–10704; b) J. Liu, M. Skaria, P. Sharma, Y.-W. Chiang, R.-S. Liu, Chem. Sci. 2017, 8, 5482–5487; c) R. Banerjee, N. J. Pace, D. R. Brown, E. Weerapana, J. Am. Chem. Soc. 2013, 135, 2497–2500; d) K.-L. Zheng, W.-M. Shu, J.-R. Ma, Y.-D. Wu, A.-X. Wu, Org. Lett. 2016, 18, 3526–3529; e) A. G. Kutateladze, J. L. Kice, T. G. Kutateladze, N. S. Zefirov, J. Org. Chem. 1993, 58, 995–996.
- [5] a) W. Yuan, X. Zhang, Y. Yu, S. Ma, Chem. Eur. J. 2013, 19, 7193–7202; b) Y. Ozawa, H. Iwamoto, H. Ito, Chem. Commun. 2018, 54, 4991–4994.
- [6] W. Zhao, J. Montgomery, J. Am. Chem. Soc. 2016, 138, 9763-9766.
- [7] R. G. Parr, Y. Weitao, Density-Functional Theory of Atoms and Molecules, Oxford University Press, 1994.
- [8] A. D. Bochevarov, E. Harder, T. F. Hughes, J. R. Greenwood, D. A. Braden, D. M. Philipp, D. Rinaldo, M. D. Halls, J. Zhang, R. A. Friesner, *Int. J. Quantum Chem.* **2013**, *113*, 2110–2142.
- [9] a) J. C. Slater, in Quantum Theory of Molecules and Solids, McGraw-Hill: New York, 1974; b) S. H. Vosko, L. Wilk, M. Nusair, Can. J. Phys. 1980, 58, 1200–1211; c) A. D. Becke, Phys. Rev. A 1988, 38, 3098–3100; d) C. Lee, W. Yang, R. G. Parr, Phys. Rev. B 1988, 37, 785–789.
- [10] S. Grimme, J. Antony, S. Ehrlich, H. Krieg, J. Chem. Phys. 2010, 132, 154104.
- [11] R. Ditchfield, W. J. Hehre, J. A. Pople, J. Chem. Phys. 1971, 54, 724–728.
- [12] a) P. J. Hay, P. Jeffrey Hay, W. R. Wadt, J. Chem. Phys. 1985, 82, 270–283; b) W. R. Wadt, P. Jeffrey Hay, J. Chem. Phys. 1985, 82, 284–298; c) P. J. Hay, P. Jeffrey Hay, W. R. Wadt, J. Chem. Phys. 1985, 82, 299–310.
- [13] T. H. Dunning, J. Chem. Phys. 1989, 90, 1007–1023.
- [14] a) B. Marten, K. Kim, C. Cortis, R. A. Friesner, R. B. Murphy, M. N. Ringnalda, D. Sitkoff, B. Honig, J. Phys. Chem. 1996, 100, 11775–11788; b) S. R. Edinger, C. Cortis, P. S. Shenkin, R. A. Friesner, J. Phys. Chem. B 1997, 101, 1190–1197; c) M. Friedrichs, R. Zhou, S. R. Edinger, R. A. Friesner, J. Phys. Chem. B 1999, 103, 3057–3061.
- [15] A. A. Rashin, B. Honig, J. Phys. Chem. 1985, 89, 5588–5593.
- [16] C. Peng, H. Bernhard Schlegel, Isr. J. Chem. 1993, 33, 449-454.
- [17] a) K. Yeung, R. E. Ruscoe, J. Rae, A. P. Pulis, D. J. Procter, *Angew. Chem. Int. Ed.* 2016, *55*, 11912–11916;
  b) Y. Huang, K. B. Smith, M. K. Brown, *Angew. Chem. Int. Ed.* 2017, *56*, 13314–13318;
  c) F. Cheng, W. Lu, W. Huang, L. Wen, M. Li, F. Meng, *Chem. Sci.* 2018, *9*, 4992–4998;
  d) H. Jang, F. Romiti, S. Torker, A. H. Hoveyda, *Nat. Chem.* 2017, *9*, 1269–1275;
  e) R. Sakae, K. Hirano, M. Miura, *J. Am. Chem. Soc.* 2015, *137*, 6460–6463;
  f) R. Corberán, N. W. Mszar, A. H. Hoveyda, *Angew. Chem. Int. Ed.* 2011, *50*, 7079–7082.
- [18] a) D. S. Laitar, P. Müller, J. P. Sadighi, J. Am. Chem. Soc. 2005, 127, 17196–17197; b) Y. Lee, A. H. Hoveyda, J. Am. Chem. Soc. 2009, 131, 3160–3161.
- [19] Y. Yang, S. L. Buchwald, Angew. Chem. Int. Ed. 2014, 53, 8677-8681.

- [20] Y. Yang, P. Liu, ACS Catal. 2015, 5, 2944–2951.
  [21] a) W. Zhao, J. Montgomery, Angew. Chem. Int. Ed. 2015, 54, 12683–12686; b) T. Jia, Q. He, R. E. Ruscoe, A. P. Pulis, D. J. Procter, Angew. Chem. Int. Ed. 2018, 57, 11305–11309.

# TOC graphic

